Current Optics and Photonics
Vol. 2, No. 4, August 2018, pp. 332-339

ISSN: 2508-7266(Print) / ISSN: 2508-7274(Online)
DOI: https://doi.org/10.3807/COPP.2018.2.4.332

Phase Error Reduction for Multi-frequency Fringe Projection Profilometry Using Adaptive Compensation

Choon Sik Cho* and Junghee Han

School of Electronics and Information Engineering, Korea Aerospace University, Goyang 10540, Korea

(Received June 18, 2018 : revised July 3, 2018 : accepted July 4, 2018)

A new multi-frequency fringe projection method is proposed to reduce the nonlinear phase error in 3-D shape measurements using an adaptive compensation method. The phase error of the traditional fringe projection technique originates from various sources such as lens distortion, the nonlinear imaging system and a nonsinusoidal fringe pattern that can be very difficult to model. Inherent possibility of phase error appearing hinders one from accurate 3-D reconstruction. In this work, an adaptive compensation algorithm is introduced to reduce adaptively the phase error resulting from the fringe projection profilometry. Three different frequencies are used for generating the gratings of projector and conveyed to the four-step phase-shifting procedure to measure the objects of very discontinuous surfaces. The 3-D shape results show that this proposed technique succeeds in reconstructing the 3-D shape of any type of objects.

Keywords : Fringe projection, Multi-frequency profilometry, 3-D reconstruction algorithm, Phase error, Adaptive compensation
OCIS codes : (100.0100) Image processing; (100.3010) Image reconstruction techniques; (100.3175) Interferometric imaging

I. INTRODUCTION

Noncontact 3-D shape measurement techniques have been extending their applications to various industrial fields such as medical, manufacturing and biometric areas. A large number of noncontact 3-D shape measurement techniques developed until now show their advantages and drawbacks as listed in [1-8]. Among them fringe projection profilometry (FPP) has been of prime interest because it provides fast operation and high resolution by using a relatively simple configuration composed of a projection system and an imaging system. The FPP technique can be classified into Fourier transform profilometry (FTP) and phase measuring profilometry (PMP) where both methods obtain the phase of objects and then provide a 3-D shape reconstruction. The FTP method shows a faster response but a lower resolution compared with the PMP method. PMP can thus be employed for the manufacturing inspection systems due to high measurement resolution, but the measurement range is restrained due to the chronic 2π ambiguity [8]. In addition, phase error occurs from the nonlinear characteristic of the measurement system configuration [9]. To resolve this issue, multi-frequency PMP is introduced to reduce the phase error by compensating the nonlinear characteristic of projection and imaging systems, and by employing the adaptive compensation based on the additive combination of sinusoidal functions [10].

Much effort for reducing the phase error in the middle of 3-D shape measurements has been expended specifically concentrating on the procedure of phase unwrapping. A mathematical model with a phase-coding method is presented for accurate phase map retrieval, but this method still illustrates unstable phase error reduction [11]. A phase measurement technique using multiple perspectives is shown but this method requires a long computation time and a complex phase map retrieval process [12]. The coded phase pattern has also been applied but this method displays a good 3-D shape measurement only for very

*Corresponding author: cscho@kau.ac.kr, ORCID 0000-0003-0833-5254
Color versions of one or more of the figures in this paper are available online.

smooth-surface objects [13]. A stair phase encoding method has been proposed showing better 3-D shape performance, but this method cannot be utilized for very discontinuous-surface objects [14, 15].

In this work, a PMP method is proposed devising an adaptive compensation technique for reducing the phase error in the process of phase retrieval for 3-D shape measurement. Since this technique capitalizes on a feedback network, the phase error is reduced repeatedly and a decision for whether the feedback should be continued or not can be made by the designers. This can be employed for very discontinuous- and rough-surface objects.

II. MULTI-FREQUENCY FRINGE PROJECTION PROFILOMETRY

Figure 1 shows the general environment of the fringe projection method. Using the projector, the fringe pattern is projected onto the object and the deformed fringe pattern is acquired through the camera. PMP is a method of obtaining the phase of an object using N sinusoidal fringe patterns with constant phase difference. The deformed fringe patterns caused by the fringe pattern projected onto the object to be measured through the projector can be obtained through the camera. Eq. (1) represents the modified fringe pattern.

$$I_n(x,y) = a(x,y) + b(x,y)\cos\left[\phi(x,y) + \frac{n\pi}{2}\right] \tag{1}$$

where $a(x,y)$ is the background intensity, $b(x,y)$ is the fringe modulation, and $\phi(x,y)$ represents the phase distribution at each point of the object. In this case, I_n depends on the number of fringe patterns used. If four fringe patterns are used, a modified fringe pattern as shown in Eq. (2) can be obtained.

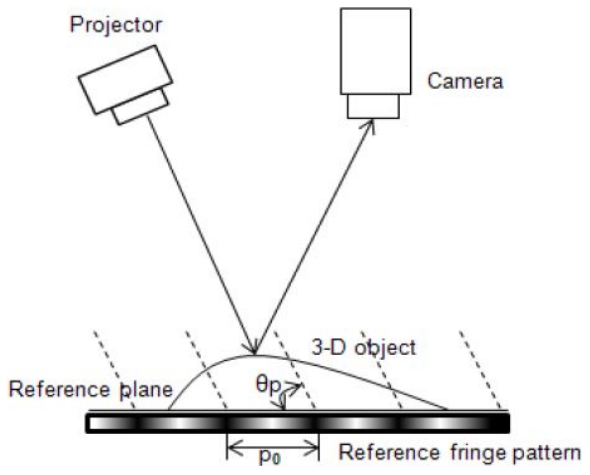

FIG. 1. The general environment for the fringe projection method.

$$\begin{aligned}
I_1(x,y) &= a(x,y) + b(x,y)\cos\left[\phi(x,y) + \frac{\pi}{2}\right] \\
I_2(x,y) &= a(x,y) + b(x,y)\cos\left[\phi(x,y) + \pi\right] \\
I_3(x,y) &= a(x,y) + b(x,y)\cos\left[\phi(x,y) + \frac{3\pi}{2}\right] \\
I_4(x,y) &= a(x,y) + b(x,y)\cos\left[\phi(x,y) + 2\pi\right]
\end{aligned} \tag{2}$$

The four modified fringe pattern formulas derived in Eq. (2) can be rewritten as in Eq. (3) using trigonometric formulas.

$$\begin{aligned}
I_1(x,y) &= a(x,y) - b(x,y)\sin\phi(x,y) \\
I_2(x,y) &= a(x,y) - b(x,y)\cos\phi(x,y) \\
I_3(x,y) &= a(x,y) + b(x,y)\sin\phi(x,y) \\
I_4(x,y) &= a(x,y) + b(x,y)\cos\phi(x,y)
\end{aligned} \tag{3}$$

Manipulating the four modified fringe patterns in Eq. (3), the phase can be calculated using Eq. (4), leading to Eq. (5).

$$\begin{aligned}
I_3(x,y) - I_1(x,y) &= 2b(x,y)\sin\phi(x,y) \\
I_4(x,y) - I_2(x,y) &= 2b(x,y)\cos\phi(x,y)
\end{aligned} \tag{4}$$

$$\phi(x,y) = \tan^{-1}\left(\frac{I_3 - I_1}{I_4 - I_2}\right) \tag{5}$$

Therefore, the phase of the object can be computed using the light intensity of each pixel of the four deformed fringe patterns obtained by photographing the fringe pattern of the deformed fringe pattern projected by the projector through the object to be measured. The actual height of the object should be calculated from the phase obtained by Eq. (5). The height of the object is calculated using the parameters described in Fig. 2.

Capitalizing the parameters shown in Fig. 2, we can obtain the height of the object. In this work, a 3D shape reconstruction system is realized by employing the PMP method that shows a relatively high resolution. In spite of this advantage, there are still problematic factors to

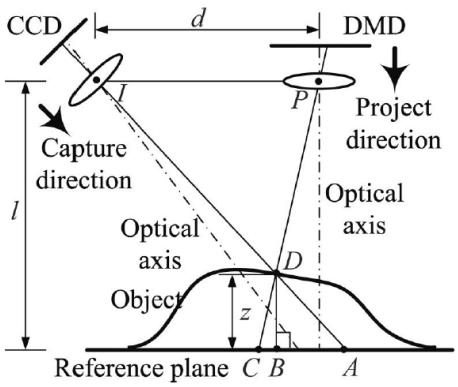

FIG. 2. Conversion from phase data to height data.

overcome. The first problem is that there is a limit to the measurement range due to ambiguity. We therefore propose a method using a multi-frequency fringe pattern to solve this problem. Secondly, we propose a method to correct the phase error by using the sum of sinusoidal functions.

We use the arctangent function as shown in Eq. (5) to obtain the phase by deciding the light intensity of the fringe pattern acquired through the camera. Due to the nature of the arctangent function, the calculation result will have a value in the range of $-\frac{\pi}{2}\sim\frac{\pi}{2}$. As a result, the height cannot fall within one wavelength of the fringe pattern, which is rapidly changing. As shown in Fig. 3, the positions C1, C2, and C3 of the objects S1, S2, and S3 having different heights are equal to each other in phase difference from the floor in the camera position. Therefore, the phase difference obtained by using the light intensity of the deformed fringe pattern is the same in all objects S1, S2, and S3 having different heights. In the fringe projection method using a single frequency, if the height of the object is not within the wavelength range of the sinusoidal fringe pattern, the problem caused by such 2π ambiguity cannot be resolved. Therefore, we propose a multi-frequency method to increase the measurement range.

The 2π ambiguity described here is the biggest problem in the process of 3D shaping with PMP. This is fundamentally very difficult to resolve with a single frequency fringe pattern. Therefore, the limitation of the measurement range which cannot be resolved by the method using the single frequency is settled by using the multi-frequency fringe pattern [15]. For a large frequency fringe pattern, it is possible to measure a precise height, but there is a disadvantage that the measurement range is small because the wavelength of the fringe pattern is short. On the other hand, the fringe pattern with a small frequency has the disadvantage that the measurement accuracy is low but the measurement range is large because of the long wavelength. Therefore, using a two-frequency fringe pattern, it is possible to maintain measurement accuracy and to widen the height range. The combination of these two advantages can resolve the 2π ambiguity.

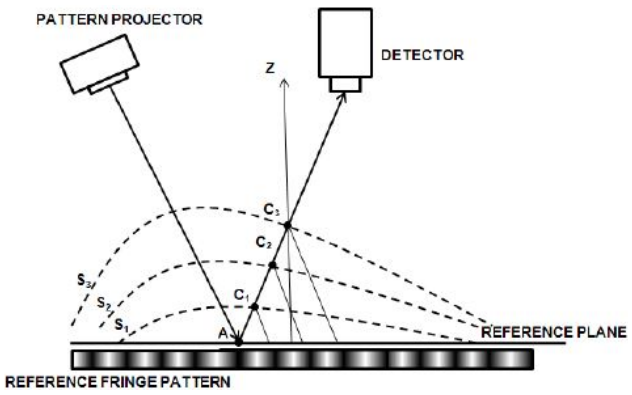

FIG. 3. 2π ambiguity.

In Fig. 4, the process of PMP using multiple frequencies is explained. For each fringe pattern with different frequencies f_1 and f_2 ($f_1 > f_2$), we can obtain the phases ϕ_1 and ϕ_2 at a single frequency using Eq. (5). Overlapping the calculated phases of f_1 and f_2 ($f_1 > f_2$) leads to the frequency difference of the fringe pattern as shown in Fig. 4. From the results in Fig. 4, we can obtain the phase using fringe patterns of f_1 and f_2 using Eq. (6).

$$\begin{aligned}\phi_{12}(x,y)&=\phi_1(x,y)-\phi_2(x,y), && \phi_1(x,y)>\phi_2(x,y)\\ \phi_{12}(x,y)&=\pi+\phi_1(x,y)-\phi_2(x,y), && otherwise\end{aligned} \tag{6}$$

The range of measurement for ϕ_{12} at one wavelength is increased when compared with the phase using a single frequency fringe pattern from ϕ_1 and ϕ_2. ϕ_{23} obtainable from ϕ_2 and ϕ_3 can also be capitalized and extended to wider range of phase, $\phi_{123,}$ which is the difference of ϕ_{12}

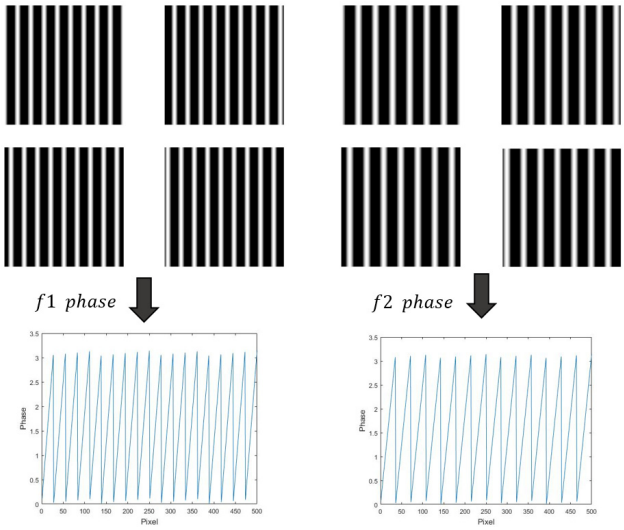

FIG. 4. The process of obtaining ϕ_1 and ϕ_2.

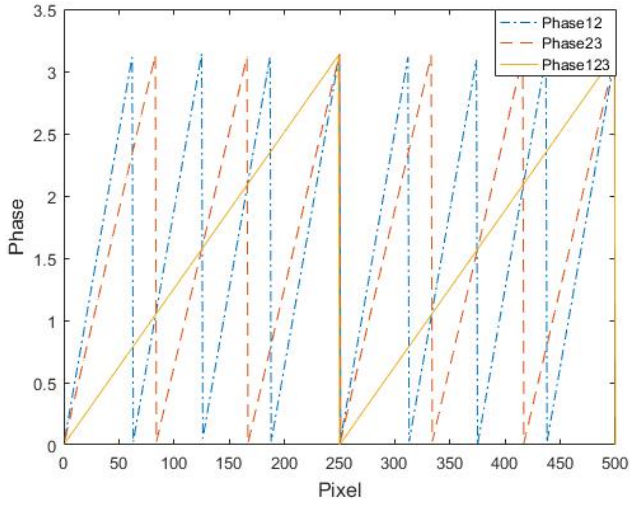

FIG. 5. The frequency difference between ϕ_1 and ϕ_2.

and ϕ_{23}, as illustrated in Fig. 5. The number of fringe patterns at different frequencies to be used can be determined by the measurement range. In the result shown in Fig. 5, it can be seen that the measurement range ϕ_{123} of the object obtained using fringe patterns for the three different frequencies of f_1, f_2 and f_3 ($f_1 > f_2 > f_3$) is increased when compared with ϕ_{12} and ϕ_{23} obtained using fringe patterns for the two frequency sets of f_1 - f_2, and f_2 - f_3, respectively ($f_1 > f_2 > f_3$).

The limitation of measurement range for object height due to the ambiguity of the single frequency PMP method can be resolved through the multi-frequency PMP described here. As the number of different fringe patterns increases, the measurement range of height increases, but it takes more time because the number of fringe patterns projected from the projector and the number of deformed fringe patterns acquired by the camera increases. In this work, three frequencies have been used.

III. MEASUREMENT RESULTS AND PHASE ERROR COMPENSATION

For an ideal 3D shape reconstruction system, the generated fringe pattern should be projected through the projector, reflected on the object to be measured, and kept constant when acquired through the camera. However, the light intensity of the fringe pattern is affected by the nonlinearity of the projector and camera. Since the fringe pattern is projected in the form of light, phase error is generated when the phase is calculated due to the influence of surrounding light. This phenomenon is explained in Fig. 6 [15].

When the generated fringe pattern (I_i) is projected through the projector, the output (I^p) is given by Eq. (7) because of the nonlinear function $f(\cdot)$ of the projector. When the fringe pattern projected forms a deformation grating in the object to be measured, it reflects in the form of Eq. (8) due to the reflectivity $r(x,y)$ of the object and ambient light of $a(x,y)$. When the object is photographed by the camera to obtain the modified fringe pattern, the finally acquired fringe pattern image due to the nonlinearity coefficient α of the camera is expressed by Eq. (9).

$$I^p(x,y) = f(I_i) \tag{7}$$

$$I^o = r(x,y)[I^p(x,y) + a(x,y)] \tag{8}$$

$$I^c(x,y) = \alpha[I^o + a(x,y)] \tag{9}$$

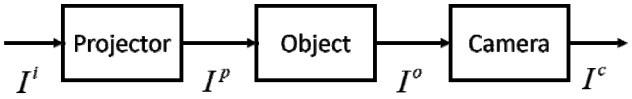

FIG. 6. The procedure for fringe pattern image processing.

The distortion of the final fringe pattern causes a phase error when calculating the phase using light intensity, yielding degradation of the accuracy of object height. This paper introduces how to correct the phase error caused by the nonlinear characteristics of projector and camera based on the fact that the intensity of light input from the camera takes originally a sinusoidal wave. Therefore, we can adaptively compensate the phase error using the curve fitting with sinusoidal waves.

Figure 7 shows the result of projecting the fringe pattern on a flat bottomed surface using the actual 3D shaping system and calculating the phase through the fringe pattern photographed by the camera. Assuming the ideal environment, the phase error in the real system can be confirmed when compared with the simulated phase. The cause of this phase error is the distortion of the fringe pattern due to nonlinearity of the projector, camera and the surrounding environment. Figure 8 shows the light intensity of the fringe pattern taken by a real camera. The fringe pattern read from the camera (I_i^C) in Eq. (9) can be simply rewritten as in Eq. (10) [14],

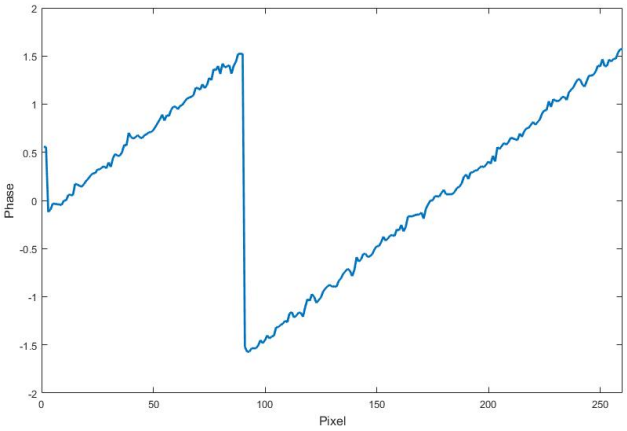

FIG. 7. Phase error in a real system.

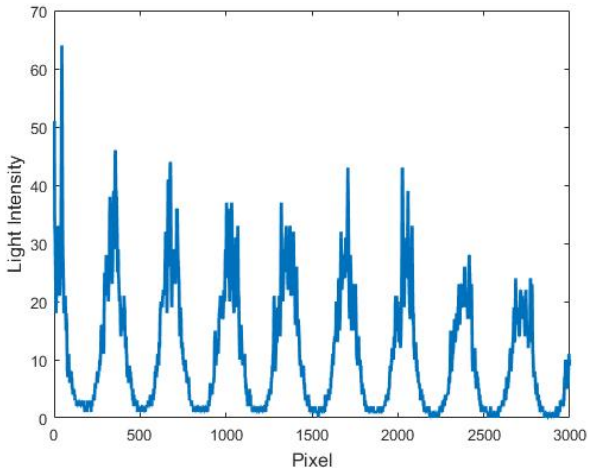

FIG. 8. Light intensity of fringe pattern photographed with a real camera.

$$\left[I_i^C\right] = r\left[I_i\right]^{\gamma_s} + I_A \tag{10}$$

where I_i is generated fringe pattern which is input to the projector, I_A is the intensity of the ambient light and r is the object reflectivity. The fringe pattern to determine the nonlinear exponent γ_s cannot be used to determine the referred light intensity since the ideal environment cannot be assumed. Therefore, each monochromatic light with different light intensity is excited at the projector, and the projected monochromatic light is photographed by the camera and analyzed to determine the nonlinear exponent. The results of three monochromatic projections I_{i1}, I_{i2} and I_{i3} are shown in Eqs. (11), (12), and (13).

$$\left[I_{i1}^C\right] = r\left[I_{i1}\right]^{\gamma_s} + I_A \tag{11}$$

$$\left[I_{i2}^C\right] = r\left[I_{i2}\right]^{\gamma_s} + I_A \tag{12}$$

$$\left[I_{i3}^C\right] = r\left[I_{i3}\right]^{\gamma_s} + I_A . \tag{13}$$

Assuming that object reflectivity and ambient light are maintained the same, the expression of eliminating the object reflectivity and the ambient light can be created as represented in Eq. (14). The nonlinear exponent can be determined for each pixel using Eq. (14).

$$\frac{\left[I_{i1}^C\right]-\left[I_{i2}^C\right]}{\left[I_{i2}^C\right]-\left[I_{i3}^C\right]} = \frac{\left[I_{i1}\right]^{\gamma_s}-\left[I_{i2}\right]^{\gamma_s}}{\left[I_{i2}\right]^{\gamma_s}-\left[I_{i3}\right]^{\gamma_s}} \tag{14}$$

The ripple of light intensity remaining after hardware correction is also a main cause of phase error. As a result, the ripple in sinusoidal waveform creates phase error. In this work, the distorted fringe pattern is modeled by combining multiple sinusoidal functions as expressed in Eq. (15). In order to reduce the phase error, the light intensity of the fringe pattern input to the camera must maintain an ideal sinusoidal shape. The fringe pattern that is initially created is an ideal single-frequency sinusoidal shape, but the projected and photographed fringe pattern cannot maintain a single frequency and phase because the projector and camera are not in ideal condition. Therefore, the shape of the photographed fringe pattern, $f(x)$, is modeled using a combination of a plurality of sine waves as shown in Eq. (15).

$$\begin{aligned} f(x) &= a_0(\cos b_0 x + c_0) + a_1(\cos b_1 x + c_1) + \ldots + a_m(\cos b_m x + c_m) \\ &= \sum_{i=1}^{m} a_i(\cos b_m x + c_m) \end{aligned} \tag{15}$$

Using the difference between the photographed fringe pattern and the modeling function as expressed in Eq. (16), we find a combination of multiple sinusoidal summations with a minimum phase error through the least squares approach.

$$[Error]^2 = (\sum_{i=0}^{m} d_i)^2 = \sum_{i=0}^{m}([I^C] - f(x_i))^2 \tag{16}$$

Figure 9 shows an adaptive compensation process using a sinusoidal sum. As the number of sine waves increases, the optimal modeling function can be found, but there is a disadvantage in the time requirement. Therefore, the

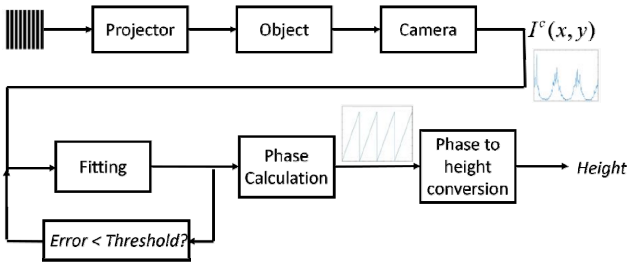

FIG. 9. Adaptive compensation process using sinusoidal sum.

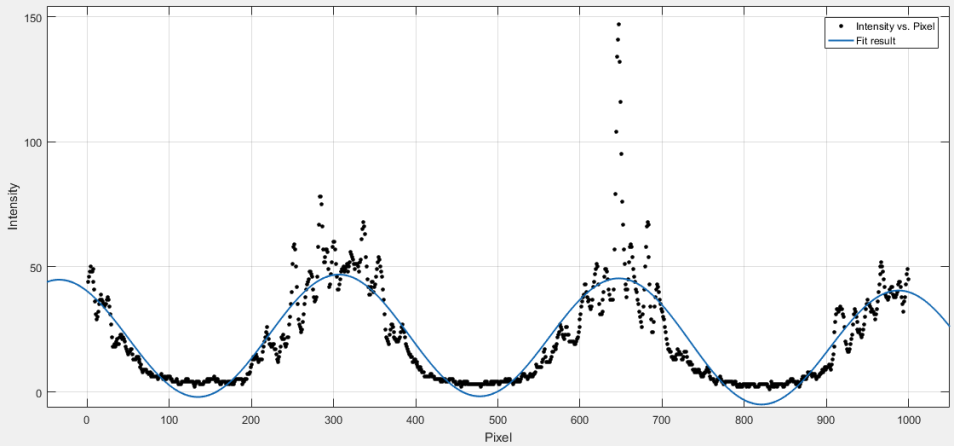

FIG. 10. Compensation result for m = 2.

maximum number of sinusoidal combinations is set to 6 in this work. Figures 10~13 show the result of modeling the fringe pattern through the aforementioned adaptive compensation process. As the number (m) of sinusoidal sum terms increases as shown in Figs. 10~13, the measured fringe pattern can be expressed more accurately using the modeling function of sine waves. Figure 13 illustrates closer modeling function compared with that of Fig. 10 as expected.

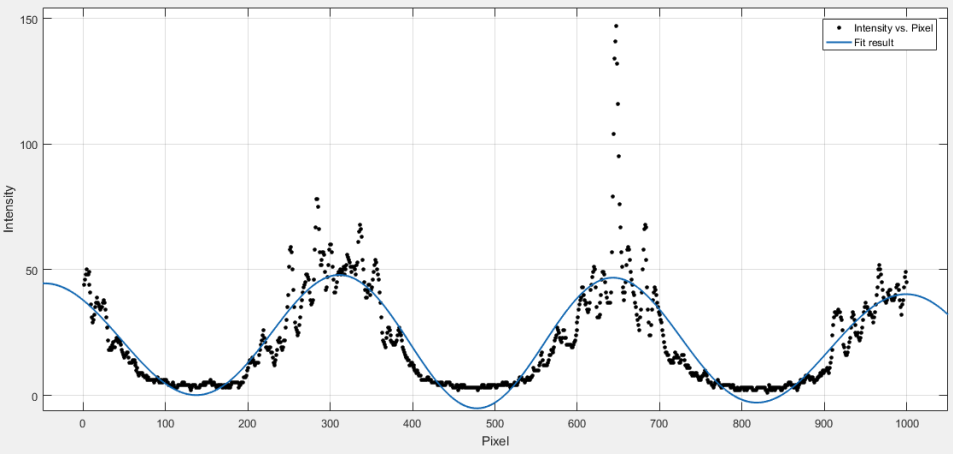

FIG. 11. Compensation result for m = 3.

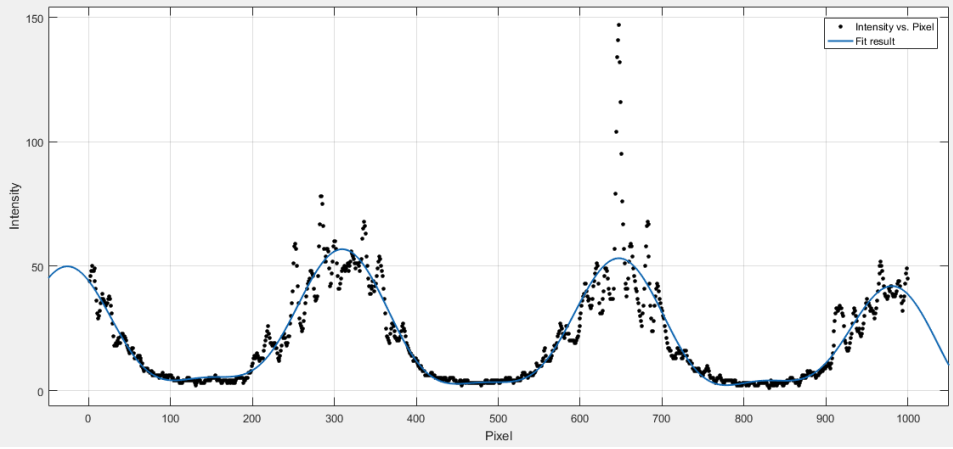

FIG. 12. Compensation result for m = 4.

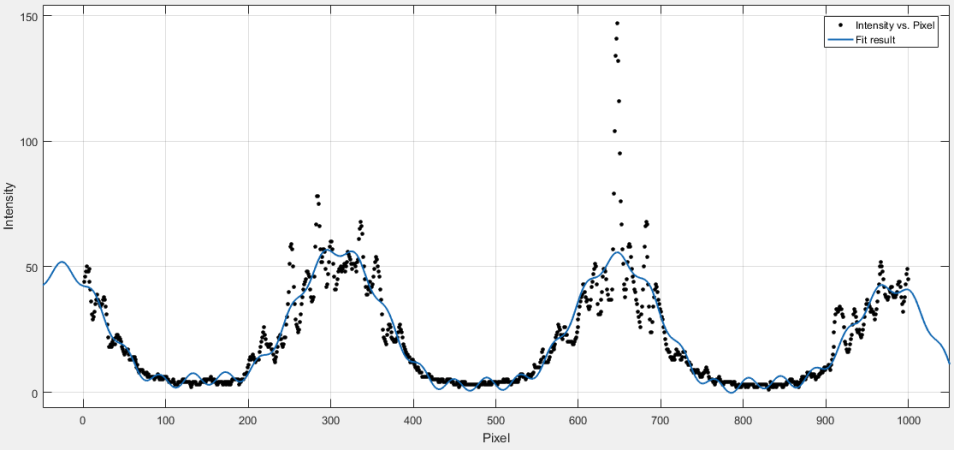

FIG. 13. Compensation result for m = 5.

A gauge block with precise height as taken in Fig. 14 is photographed using three frequencies. As shown in Fig. 14, the vertical and horizontal gauge blocks are maintained and the experiment is conducted. Phase error compensation proposed here is applied to this gauge block and analyzed.

Now, we compare the results of 3D shaping after hardware and phase error compensations with those before phase error compensation. Figure 15 shows the 3D shape of the gauge block before the phase error compensation and Fig. 16 shows that after the phase error compensation.

FIG. 14. Gauge block used for 3-D shaping.

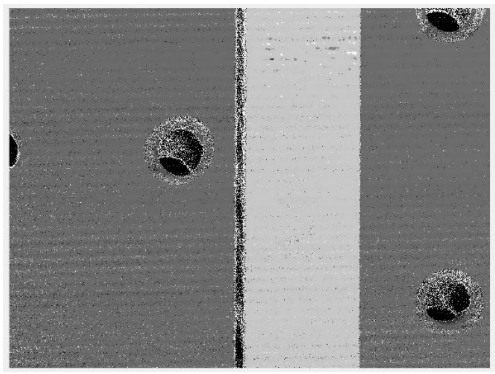

FIG. 15. 3D shaping of gauge block before phase error compensation.

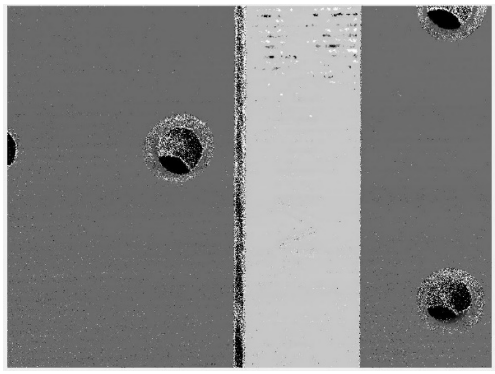

FIG. 16. 3D shaping of gauge block after phase error compensation.

As shown in Fig. 16, the surface has become significantly smoother compared with that of Fig. 15 since the noisy surface has been corrected successfully using the phase error compensation. Therefore, 3D shaping with phase error compensation can be clearer than without it. Figure 17 represents the results before and after phase error compensation. Table 1 numerically shows the phase error before and after the phase error correction. In order to numerically evaluate the improvement after the phase error correction, phase error at each pixel is squared and the sums before

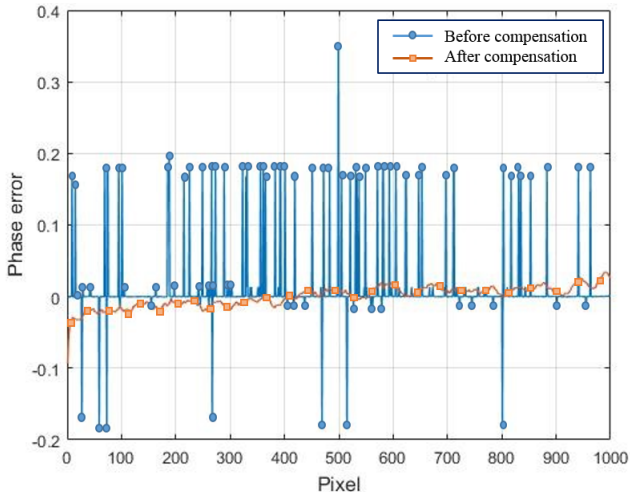

FIG. 17. Comparison of phase error before and after compensation.

TABLE 1. Phase errors before and after phase error compensation

	Phase error before compensation		Phase error after compensation	
Pixel	Error	$(Error)^2$	Error	$(Error)^2$
200	0.0103	0.000106	-0.0605	0.00366
400	-0.1813	0.03287	0.0805	0.00648
600	0.1812	0.032833	-0.0322	0.001037
800	0.1132	0.012814	-0.0922	0.008501
1000	0.2132	0.045454	0.0626	0.003919
1200	0.2494	0.0622	-0.032	0.001024
1400	0.1683	0.028325	-0.058	0.003364
1600	-0.1811	0.032797	-0.0214	0.000458
1800	0.2078	0.043181	-0.0201	0.000404
2000	-0.011	0.000121	0.0387	0.001498
2200	0.1208	0.014593	0.015	0.000225
2400	0.1283	0.016461	-0.0227	0.000515
2600	0.3678	0.135277	0.372	0.138384
2800	0.0129	0.000166	-0.0362	0.00131
	Sum	0.457199	Sum	0.170779

TABLE 2. Measured results for the height of a gauge block

Nominal (mm)	Before compensation (mm)	After compensation (mm)	Error (μm)	%Error
1.5	1.505	1.5020	2.615	0.174
1.6	1.609	1.6068	2.555	0.159
1.7	1.707	1.7037	3.123	0.183
1.8	1.812	1.8082	4.042	0.224
1.9	1.916	1.9112	4.788	0.251
2	2.027	2.0190	7.702	0.381

and after compensation are compared. As a result, the phase error reduction rate after the phase error correction approaches 92.64%. Table 2 shows the results of measuring the height of a gauge block. Since the gauge block is manufactured with precise dimensions, it is a tool to measure height accuracy before and after phase error compensation. If the phase error is compensated, the height of the object can be measured more precisely. This is because the phase error is related to the depth of the object to be measured. The smaller the phase error, the smaller the amount of ripples present on the surface of the object, and thus the more accurately the height data can be measured.

IV. CONCLUSION

In this paper, we developed a 3D shape reconstruction system using a multi-frequency phase measuring profilometry method with improved phase error using adaptive compensation. It is confirmed that the limitation of measurement range in the single frequency method is resolved by using multiple frequencies. In addition, the error reduction rate of 92.64% was obtained when modeling fringe pattern by combination of hardware correction and sinusoidal wave compared with that before phase error correction. It is confirmed that it is possible to measure more accurate height data by compensating the phase error associated with the depth problem of the object height data. This is proved by gauge block measurement of precise dimensions and it is suitable for use as inspection equipment in various fields of industry by showing the 3D shape of a complex object.

REFERENCES

1. G. Sansoni, M. Trebeschi, and F. Docchio, "State-of-the-art and applications of 3D imaging sensors in industry, cultural heritage, medicine, and criminal investigation," Sens. **9**, 568-601 (2009).
2. H. Takasaki, "Moiré topography," Appl. Opt. **9**, 1467-1472 (1970).
3. O. Kafri and I. Glatt, *The Physics of Moiré Metrology* (John Wiley & Sons, NJ, USA, 1990).
4. I. Amidror, *The Theory of the Moiré Phenomenon* (Kluwer Academic Publishers, Dordrecht, Netherlands, 2000).
5. N. Li, "Simulation of a small feature gauging system using phase-shift projection Moiré topography," in *Proc. IEEE International Conference on Information Management and Engineering* (China, Apr. 2010), pp. 366-369.
6. J. Degrieck, W. Van Paepegem, and P. Boone, "Application of digital phase shift shadow Moiré to micro deformation measurement of curved surface," Opt. Lasers Eng. **36**, 29-40 (2001).
7. G. S. Spagnolo, D. Ambrosini, and D. Paoletti, "Low-cost optoelectronic system for three-dimensional artwork texture measurement," IEEE Trans. Image Process. **13**, 390-396 (2004).
8. K. Wenzel, A. Antal, K. Molnar, B. Toth, and P. Tamas, "New optical equipment in 3D surface measuring," J. Autom., Mobile Rob. Intell. **3**, 29-32 (2009).
9. K. Liu, Y. Wang, D. L. Lau, Q. Hao, and L. G. Hassebrook, "Gamma model and its analysis for phase measuring profilometry," J. Opt. Soc. Am. A **27**, 553-562 (2010).
10. M. Takeda, H. Ina, and S. Kobayashi, "Fourier-transform method of fringe-pattern analysis for computer-based topography and interferometry," J. Opt. Soc. Am. **72**, 156-160 (1982).
11. D. C. Ghiglia and M. D. Pritt, *Two-Dimensional Phase Unwrapping: Theory, Algorithms, and Software* (John Wiley & Sons, NJ, USA, Wiley, 1998).
12. H. Zhao, W. Chen, and Y. Tan, "Phase-unwrapping algorithm for the measurement of three-dimensional object shapes," Appl. Opt. **33**, 4497-4500 (1994).
13. S. Zhang and P. S. Huang, "Phase error compensation for a 3-D measurement system based on the phase-shifting method," Opt. Eng. **46**, 063601 (2007).
14. C. Zhou, T. Liu, S. Si, J. Xu, Y. Liu, and Z. Lei, "An improved stair phase encoding method for absolute phase retrieval," Opt. Lasers Eng. **66**, 269-278 (2015).
15. Z. Lei, C. Wang, and C, Zhou, "Multi-frequency inverse-phase fringe projection profilometry for nonlinear phase error compensation," Opt. Lasers. Eng. **66**, 249-257 (2015).